Gastro Hep Advances 2023;2:261–276

ORIGINAL RESEARCH—BASIC

Age-dependent Microglial Disease Phenotype Results in Functional Decline in Gut Macrophages

Estelle Spear Bishop,[1,§] Hong Namkoong,[1,§] Laure Aurelian,[2,3] Madison McCarthy,[4] Pratima Nallagatla,[5] Wenyu Zhou,[5,6] Leila Neshatian,[1] Brooke Gurland,[4] Aida Habtezion,[1,*] and Laren Becker[1,*]

[1]Division of Gastroenterology and Hepatology, Department of Medicine, Stanford University, Stanford, California; [2]Stanford University School of Medicine OFDD, Stanford, California; [3]Department of Pharmacology, University of Maryland School of Medicine, Baltimore, Maryland; [4]Department of Surgery, Stanford University, Stanford, California; [5]Stanford Center for Genomics and Personalized Medicine, Stanford University, Stanford, California; and [6]Department of Genetics, Stanford University, Stanford, California

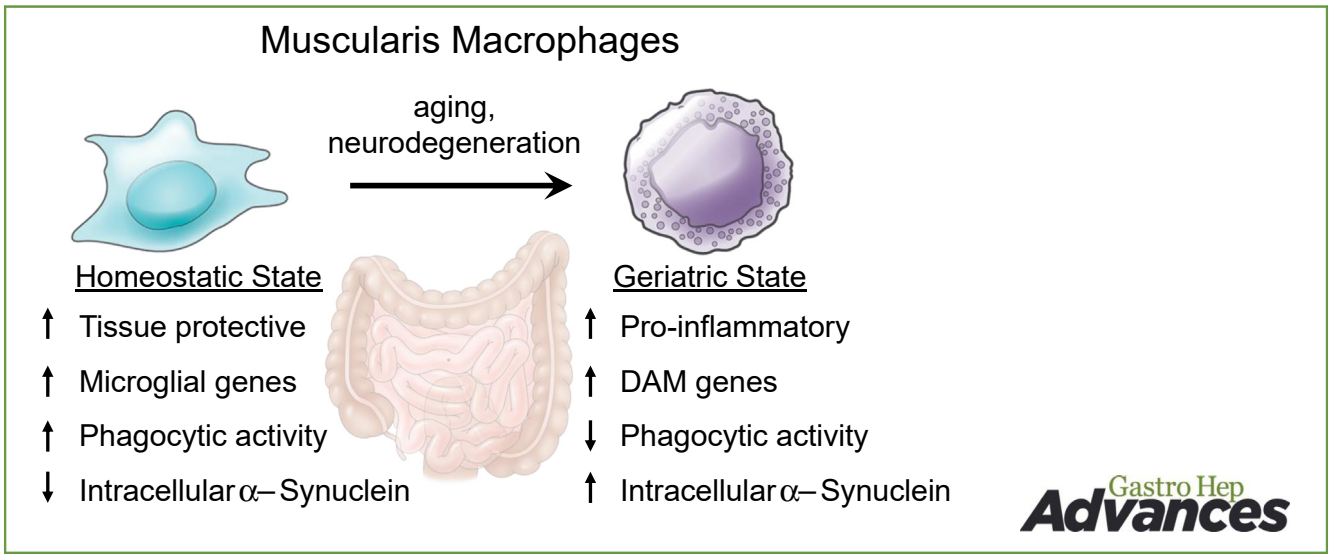

BACKGROUND AND AIMS: Muscularis macrophages (MMs) are tissue-resident macrophages in the gut muscularis externa which play a supportive role to the enteric nervous system. We have previously shown that age-dependent MM alterations drive low-grade enteric nervous system inflammation, resulting in neuronal loss and disruption of gut motility. The current studies were designed to identify the MM genetic signature involved in these changes, with particular emphasis on comparison to genes in microglia, the central nervous system macrophage population involved in age-dependent cognitive decline. **METHODS:** Young (3 months) and old (16–24 months) C57BL/6 mice and human tissue were studied. Immune cells from mouse small intestine, colon, and spinal cord and human colon were dissociated, immunophenotyped by flow cytometry, and examined for gene expression by single-cell RNA sequencing and quantitative real-time PCR. Phagocytosis was assessed by in vivo injections of pHrodo beads (Invitrogen). Macrophage counts were performed by immunostaining of muscularis whole mounts. **RESULTS:** MMs from young and old mice express homeostatic microglial genes, including *Gpr34*, *C1qc*, *Trem2*, and *P2ry12*. An MM subpopulation that becomes more abundant with age assumes a geriatric state (GS) phenotype characterized by increased expression of disease-associated microglia genes including *Cd9*, *Clec7a*, *Itgax* (CD11c), *Bhlhe40*, *Lgals3*, *IL-1β*, and *Trem2* and diminished phagocytic activity. Acquisition of the GS phenotype is associated with clearance of α-synuclein aggregates. Human MMs demonstrate a similar age-dependent acquisition of the GS phenotype associated with intracellular α-synuclein accumulation. **CONCLUSION:** MMs demonstrate age-dependent genetic changes that mirror the microglial disease-associated microglia phenotype and result in functional decline.

***co-senior authorship. §Dual first authorships.**

Abbreviations used in this paper: **α-SYN, α-synuclein; BCS, bovine calf serum; DAM, disease-associated microglia; DCs, dendritic cells; ENS, enteric nervous system; FACS, fluorescent-activated cell sorting; GS, geriatric state; HBSS, Hank's Buffered Saline Solution; HS, homeostatic state; LpM, lamina propria macrophage; MM, muscularis macrophage; MFI, mean fluorescence intensity; NAMs, nerve-associated macrophages; PBS, phosphate-buffered saline; PD, Parkinson's disease; PFA, paraformaldehyde; qPCR, quantitative real-time PCR; scRNA-seq, single-cell RNA sequencing.**

Most current article

2772-5723
https://doi.org/10.1016/j.gastha.2022.09.006

Keywords: Enteric Nervous System; Muscularis Macrophages; Microglia; Aging

Introduction

Muscularis macrophages (MMs) are tissue-resident macrophages located in the gut muscularis externa in close proximity to enteric neurons which play a supportive role to the enteric nervous system (ENS). MMs sense cues in the ENS microenvironment including those from neurons and the gut microbiota and relay the information to neighboring enteric neurons and smooth muscle cells.[1–8] Unlike macrophages from the mucosal gut layer (termed lamina propria macrophages [LpMs]) that preferentially express proinflammatory associated genes (M1 phenotype), MMs display an anti-inflammatory M2 phenotype.[1] Alterations in the MM phenotype have been implicated in gastrointestinal (GI) motility disorders, including gastroparesis, postinfectious GI dysmotility, and postoperative ileus,[6,8–13] and experimental MM depletion causes apoptosis of enteric neurons and disruption in gut motility.[2,14] We have previously shown that aging causes a shift in MM phenotype from anti-inflammatory to proinflammatory, resulting in neuroinflammation that is associated with apoptosis of enteric neurons and disruption of gut motility.[15] However, whether these age-dependent functional alterations affect all MMs uniformly or just a subset and the mechanism behind such changes remain poorly understood.

Tissue-resident macrophages associated with peripheral nerves share common functions and genetic signatures with microglia, the macrophage population in the central nervous system.[14,16–19] The present studies were stimulated by the finding that microglia play a central role in age-related cognitive changes.[20] Indeed, a microglial subpopulation in aged animals is characterized by diminished expression of genes involved in normal homeostatic cell functions and increased expression of disease-associated microglia (DAM) genes that are involved in pattern recognition, phagocytosis, and leukocyte adhesion.[21–25] We report that murine and human MMs express a microglial gene profile that changes with aging. MMs from aged animals express geriatric state (GS) genes that are similar to the microglial DAM genes. GS genes in both mouse and human MMs are induced by the intracellular accumulation of α-synuclein (α-SYN).

Methods

Further details are provided in Supplemental Materials.

Animals

Specific pathogen-free C57BL/6 mice (3, 10, and 16–29 months old) were acquired from the National Institute on Aging aged rodent colony. All mice were housed in temperature- and humidity-controlled rooms with a 12-hour light-dark cycle and maintained on ad libitum standard chow and water. Animal handling and procedures followed the National Institutes of Health Statement of Compliance with Standards for Humane Care and Use of Laboratory Animals and were approved by the Stanford University Institutional Animal Care and Use Committees.

Table 1. Patient Characteristics

Patient#	Sex	Age	Colon site	Indication
1	M	41	Sigmoid	Colon CA
2	M	65	Left colon	Rectal CA/diverticular disease
3	F	56	Left colon	STC
4	F	71	Rectosigmoid	Diverticular disease
5	M	74	Left colon	Sigmoid volvulus
6	F	73, 74	Sigmoid	Rectal prolapse
7	F	49	Sigmoid	Rectal prolapse
8	F	47	Left colon	STC
9	F	92	Sigmoid	Rectal prolapse
10	M	65	Left colon	Diverticular disease
11	M	86	Sigmoid	Rectal CA (neoadjuvant XRT)
12	F	50	Sigmoid	Colon CA
13	F	92	Rectosigmoid	Rectal prolapse
14	M	50	Sigmoid	Adhesive mesh
15	F	25	Sigmoid	Rectal prolapse
16	F	68	Rectosigmoid	Rectal prolapse
17	F	88	Sigmoid	Rectal CA
18	F	53	Rectosigmoid	Rectal prolapse
19	F	74	Sigmoid	Diverticular disease
20	F	88	Sigmoid	Rectal prolapse
21	F	95	Sigmoid	Rectal prolapse
22	F	75	Sigmoid	Rectal prolapse
23	F	70	Sigmoid	Rectal prolapse
24	M	84	Sigmoid	Sigmoid volvulus
25	F	57	Sigmoid	Rectal prolapse
26	F	82	Sigmoid	Sigmoid volvulus

Patient 6 had surgery twice for rectal prolapse.
CA, cancer; F, female; M, male; STC, slow transit constipation; XRT, radiation therapy.

Human Samples

All colon resection samples were obtained under an institutional review board (IRB)-approved study at Stanford Hospital (IRB-55435, IRB-11977). Full-thickness colon specimens were obtained from patients undergoing colorectal surgery for indications including cancer, rectal prolapse, diverticular disease, constipation, and volvulus (Table 1). For rectal prolapse cases, the most proximal part of the resected bowel was taken. For cancer cases, normal tissue margins, confirmed by histologic examination by a trained pathologist, were included in the study. Tissue was placed in freezing media (Roswell Park Memorial Institute media with 80% fetal bovine serum and 10% dimethyl sulfoxide) or embedded in optimal cutting temperature compound (after fixation in 4% paraformaldehyde [PFA] and incubation in 30% sucrose) and stored at -80 °C until further processing.

Antibodies and Reagents

Antibodies used in flow cytometry and immunofluorescent staining are listed in Table A1. Media and reagents are listed in Table A2.

Tissue and Cell Preparation

Mice were euthanized, and laparotomy was performed. The small intestine (SI) and colon were removed and lavaged, and the muscularis externa was dissected and fixed in 4% PFA for whole-mount preparations or enzymatically digested with collagenase and dispase, as previously described.[15] Following the removal of the muscularis externa, the remaining lamina propria tissue was incubated with stirring (20 minutes; 37 °C) in Hank's Buffered Saline Solution (HBSS) with 2% bovine calf serum (BCS) and 2-mM ethylenediaminetetraacetic acid to deplete epithelial cells. After washing in phosphate-buffered saline (PBS), the tissue was enzymatically digested in collagenase and dispase, mechanically dissociated by gentle trituration, and filtered through a 100-μm nylon mesh cell strainer for single-cell preparation. For spinal cord cell isolation, the vertebral column was removed, and a 20G needle containing 10 mL of 1X PBS was inserted into the lumbar vertebral foramen for ejection of the intact spinal cord by irrigation. The spinal cord was sectioned into small pieces and enzymatically digested with collagenase and dispase, mechanically dissociated by gentle trituration, and filtered through a 100-μm nylon mesh cell strainer. Mononuclear cells were enriched (and myelin debris removed) by centrifugation in a Percoll gradient.[26]

For human tissue, following the dissection of muscle and mucosa layers, mucosal tissue was incubated with stirring (20 minutes × 2; 37 °C) in HBSS with 2% BCS and 2-mM ethylenediaminetetraacetic acid to deplete epithelial cells. After washing in PBS, muscularis and lamina propria were minced and enzymatically digested (30 minutes, 37 °C [lamina propria]; 45 minutes, 37 °C [muscle] with spinning at 400 rpm) in an Roswell Park Memorial Institute digestion buffer containing 5% BCS , 10-mM 4-(2-hydroxyethyl)-1-piperazineethanessulfonic acid buffer, 0.25-mg/ml Liberase TL (Roche, Basel, Switzerland) and 20-U/ml DNase I. Cells were filtered through a 100-μm nylon mesh cell strainer for single-cell preparation.

Single-Cell Transcriptomics

$CD45^+$-sorted cells were subjected to droplet-based 3′-end massively parallel single-cell RNA sequencing (scRNA-seq) using Chromium Single Cell 3′ version 3 library kits (10x Genomics), as per manufacturer's instructions. The libraries were sequenced using an Illumina HiSeq 4000 Sequencing System, with 3 pooled libraries on 1 lane. Sample demultiplexing, barcode processing, single-cell counting, and reference genome mapping (refdata-cellranger-mm10–3.0.0) were performed using the Cell Ranger Single-Cell Software Suite (10x Genomics) according to the manual. The average total reads sequenced per sample were 110,059,643. An average of 87.6% of the reads were mapped to reference genome, which results in an average of 2517 genes/cell sequenced in 488 cells/sample (Table A3). Young and old samples were normalized to present the same effective sequencing depth by using the Cell Ranger aggr function. The dimensionality reduction by the principal components analysis, the graph-based clustering using the K-means algorithm, and t-distrubuted stochastic neighboring embedding visualization were performed using Cell Ranger. The cluster heat map analysis was performed using the "NormalizeData" and "AverageExpression" functions in Seurat 3.0.

Flow Cytometry and Immunofluorescent Staining

Muscularis externa was fixed in 4% PFA for immunofluorescent staining or enzymatically digested with collagenase and dispase for flow cytometry.[4,15] For flow cytometry, the dissociated cells were treated with 5% rat serum and the mouse anti-CD16/CD32 antibody in fluorescent-activated cell sorting (FACS) buffer (HBSS containing 2% BCS) for 20 minutes at 4 °C for mouse cells or 2% mouse serum and a Fc-Receptor blocking solution for 15 minutes at room temperature for human cells. Cells were incubated with primary antibodies (Table A1) or fluorescence minus one controls (30 minutes at 4 °C). 4′,6-diamidino-2-phenylindole was used for live/dead cell determination. For intracellular α-SYN staining, cells were first treated (10 minutes, 4 °C) with Zombie Aqua (Biolegend, San Diego, CA) for determining cell viability, followed by blocking and subsequent incubation (20 minutes, 4 °C) with antibodies for cell surface immune markers (Table A1). The cells were subsequently fixed and permeabilized using the eBioscience Transcription Factor Staining Buffer Kit (as per manufacturer's protocol) and stained with the Alexa Fluor 488-conjugated α-SYN antibody (Abcam, Boston, MA). After washing with the FACS buffer, the cells were passed through a 40-μm nylon mesh cell strainer prior to the FACS analysis (BD LSRII; BD Biosciences, San Jose, CA) or cell sorting (BD Aria) into Dulbecco's Modified Eagle Medium containing 10% fetal bovine serum (for single-cell transcriptomics) or QIAzol (QIAGEN, Redwood City, CA) (for quantitative real-time PCR [qPCR]). The analysis was performed using the FlowJo Software (Tree Star Inc, Ashland, OR), and the results are expressed as signal intensity calculated by the mean fluorescence intensity (MFI). For immunofluorescence, a piece of mid-SI muscularis tissue (corresponding to jejunum) was permeabilized, blocked, and incubated with primary antibodies (2 days, 4 °C) followed (overnight, 4 °C) by fluorescently labeled secondary antibodies (Table A1) and imaged with a Nikon C1 cooled charge-coupled device camera confocal microscope as previously described.[15]

RNA Isolation and Quantitative Real-Time PCR

RNA isolation and qPCR were performed as previously described[4,15] using TaqMan probes and primers listed in Table A4. The relative expression between groups was analyzed using the Pfaffl method.[27]

Microinjections of pHrodo Beads

To evaluate the phagocytosis ability of macrophages, muscularis microinjection was performed in young (5–8 weeks, n = 8) or old (22–24 weeks, n = 11) male mouse colons using pHrodo Green Zymosan Bioparticles Conjugate (Invitrogen). The mice were anesthetized with isoflurane, and a laparotomy was performed. pHrodo Bioparticles (1 mg/ml) were injected into 5 sites (5 μL/site) of the muscularis externa between the proximal and middle portions of the colon using a 10-μL Gastight Syringe (Hamilton, 7653-01) equipped with a 34-gauge small hub RN needle (Hamilton, 207,434-10). The abdomen was sutured, and the mice were sacrificed after 1 hour. The colon was removed and lavaged, and the muscularis externa was dissected and enzymatically digested in 3 mL of collagenase and dispase during incubation in a water bath at 37 °C. After washing in PBS, the tissue was enzymatically digested in collagenase and dispase, mechanically dissociated by gentle trituration, and filtered through a 100-μm nylon mesh cell strainer for single-cell preparation.

Human Immunofluorescent Staining

Full-thickness human colon samples approximately 1 cm × 0.5 cm in length were fixed in 4% PFA and then cryopreserved

by immersion in 30% sucrose. The tissue was embedded in a Tissue-Tek optimal cutting temperature (Sakura, Hayward, CA) compound and frozen at −80 °C. The frozen tissue was sectioned at a thickness of 10 μM on a Leica Cryostat (CM 1950), mounted onto coated slides, and stored at −80 °C until staining. On the day of staining, the slides were thawed and air-dried, and the tissue was circled with a hydrophobic PAP pen. Following rehydration in PBS, the tissue was permeabilized in 2% Triton-x 100 (Sigma) with 1% goat serum for 15 minutes, followed by blocking in 10% goat serum for 1 hour. The samples were incubated overnight in a humidified chamber at 4 °C with primary antibodies followed by a room temperature (1 hour) incubation with secondary antibodies (Table A1). The tissue was cover-slipped using a 4',6-diamidino-2-phenylindole mounting medium (VECTASHIELD H-1200, Vector Labs, Newark, CA). Slides were imaged on a Keyence BZ-X800 microscope at 40x magnification. Z-stack images were acquired using the optical sectioning function at a stack height of 0.6 μM (BZ-X800 Viewer), and one representative plane was selected by implementing full focus (BZ-X800 Analyzer).

Quantification and Statistical Analyses

For α-SYN quantification, the number of cells costaining with antibodies to major histocompatibility complex class II (MMs) and α-SYN were counted in 10 randomly selected fields containing enteric ganglia using a 60X objective. A minimum of 8 fields and 30 MMs (range 30-106, average 63) were analyzed per animal. Data are expressed as mean ± standard error of the mean and analyzed using *t*-test, one-way analysis of variance with Bonferroni's multiple comparisons test, two-way analysis of variance with a two-stage linear step-up procedure, simple linear regression, and Pearson correlation as detailed in the figure legends. A statistical analysis was performed with GraphPad Prism 9 (GraphPad Software Inc, La Jolla, CA), and significance was established at $P < .05$. A differential analysis of the scRNA-seq data used Seurat 3.0 with "NormalizeData" and "FindMarkers" functions.[28] The data from old and young mice were compared using the Wilcoxon rank-sum method, and $P < .05$ was used for significance after multiple hypotheses corrections by the Benjamini-Hochberg method.[29]

Results

MMs Share a Genetic Signature With Microglia and Peripheral Nerve-Associated Macrophages

$CD45^+$ cells from SI muscularis externa tissue of young (3 months, n = 2) and old (24 months, n = 3) male C57BL/6 mice were isolated by flow cytometry and examined for gene expression by scRNA-seq using drop-seq methods (Figure 1A). An unbiased t-distrubuted stochastic neighboring embedding plot analysis of 1705 cells by k-means clustering identified 5 cell clusters in both young and old mice (Figure 1B and C). These clusters were assigned as MMs (*Cd163*, *Cd14*; cluster 1), T cells (*Cd3*, *Thy1*, *T cell receptor beta* (*Tcrb*); cluster 2), immature B cells (*Cd19*, *Cd79a*; cluster 3), and mature B cells (*Ighg2b*, *Ighm*, *Jchain*; cluster 4) based on the expression of known marker genes (Figure 1D). Cluster 5 did not reflect a presently identifiable immune cell population. Old mice had a higher proportion of cells in cluster 2 (T cells) and a lower proportion in cluster 1 (MMs) (Figure 1C), consistent with our prior observations in young and old mice.[15]

The MMs (cluster 1) expressed several homeostatic microglial genes[25] including *C1qa*, *C1qb*, *C1qc*, *C3ar1*, *Cx3cr1*, *Fcgr1*, *Mafb*, *P2ry6*, and *Trem2* (highlighted in red in Figure 1D) and genes in common with other peripheral nerve-associated macrophages (NAMs)[18,19] including *Cbr2*, *Ccl12*, and *Ms4a7* (highlighted in blue in Figure 1D). Expression of these genes was similarly enriched in MMs from both young and old mice (Figure A1A). Similar to other peripheral NAMs,[18,19] MMs did not exhibit increased expression of *Sall1* (Figure A1B), a transcription factor important for the microglial function,[30] suggesting that while similar to microglia, MMs maintain a genetic signature unique to their microenvironment.

To validate our single-cell transcriptomics data, $CD45^+F4/80^+CD11b^+$ cells isolated from SI muscularis (MMs), SI mucosa (LpMs), and spinal cord (microglia) of young mice (3 months, n = 9) (Figure 1E) were evaluated for expression of several homeostatic microglial genes. Expression of the microglial purinergic receptor P2ry12[25] was significantly higher ($P < .001$) in MMs than in LpMs by cell surface and RNA expression (Figure 1F and G). MMs also had a significantly reduced ($P < .001$) expression of CD45 compared to LpMs (Figure 1F), further reflecting their similarity to microglia, which have low levels of CD45 expression.[31] Expression of the homeostatic microglial genes *Trem2*, *Cx3cr1*, *Gpr34*, *Mef2a*, and *Hexb* was significantly higher (adjusted $P < .001$) in MMs than in LpMs in both young and old (26 months, n = 6) mice (Figure 1G, Figure A1C), consistent with prior reports of microglia-specific gene expression in subsets of gut macrophages.[14,32,33] To determine if this microglial genetic signature was unique to SIs, homeostatic microglial gene expression was compared in MMs from SI and colon. Except for *Trem2*, which was elevated in MMs from colon compared to SI, the expression profile of homeostatic microglial genes did not differ (Figure A1D), suggesting this microglial genetic signature is common to MMs throughout the gut. To evaluate if sex influences expression of microglial genes, SI MMs were compared between male and female mice (3 months, n ≥ 5/group). MMs from female mice exhibited higher expression of several homeostatic microglial genes than those from males, including *P2ry12*, *Trem2*, *Cx3cr1*, *Gpr34*, and *Mef2a* (Figure A1E). Collectively, these data indicate that MMs from SI and colon of both sexes share a genetic signature with microglia and peripheral NAMs.

MMs Acquire a Microglial DAM-Like Phenotype With Aging

To examine the contribution of aging to MM gene expression, scRNA-seq data from MMs of 3- and 24-month-old male mice were subjected to an unbiased subcluster analysis using the K-means algorithm. In both age groups, the MM cluster (cluster 1, Figure 1A) segregated into 2 subclusters (1A and 1B) (Figure 2A), but the 1B/1A ratio (calculated per mouse) was significantly higher ($P = .03$) in the old mice than that in the young mice (Figure A2A).

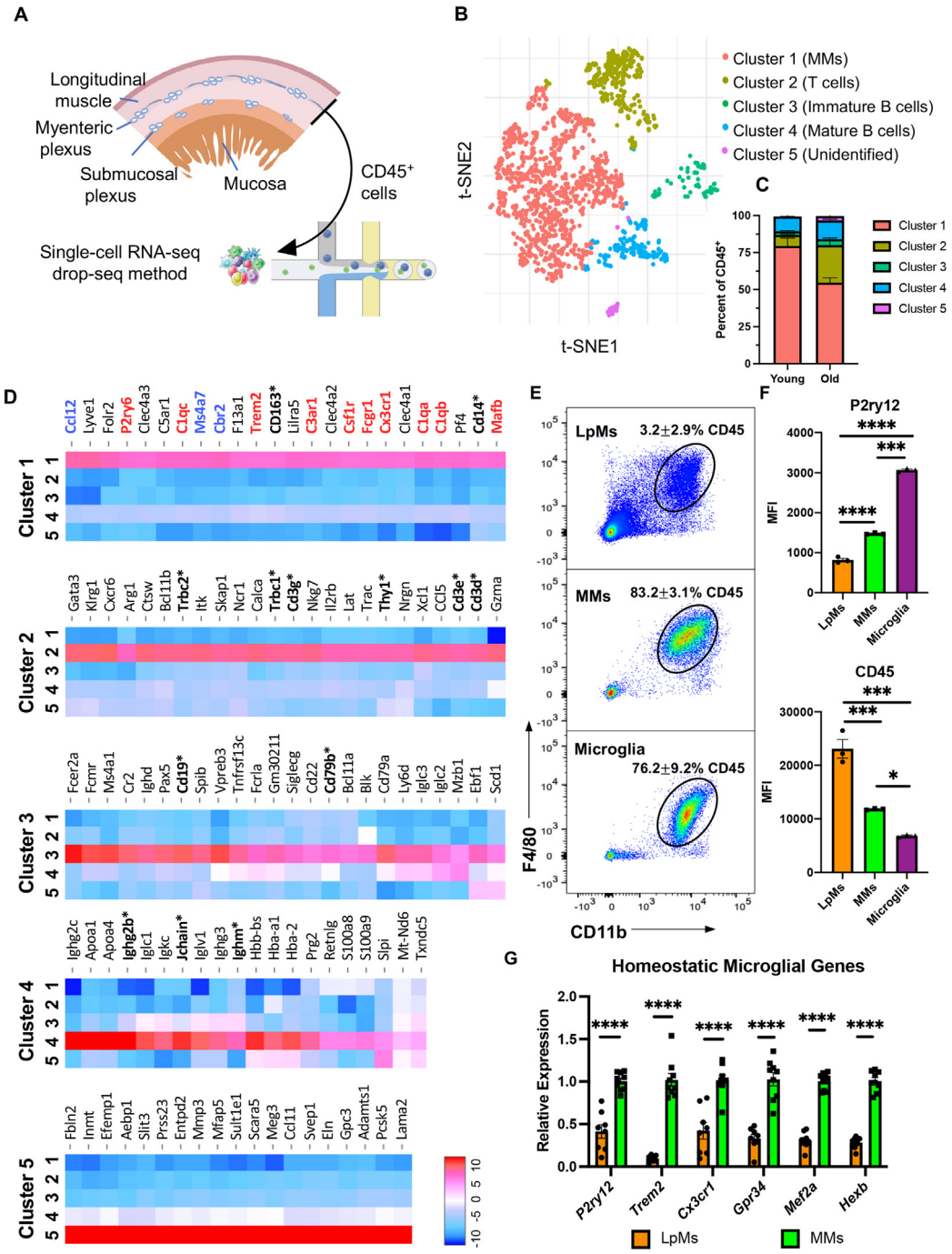

Figure 1. Transcriptional profile of CD45$^+$ cells in SI muscularis. (A) Schematic diagram of CD45$^+$ cell isolation and single cell transcriptomics from small intestine (SI) muscularis [modified from 10X Genomics User Guide (July 25, 2019) and created with BioRender.com]. (B) t-distrubuted stochastic neighboring embedding (t-SNE) plot of the scRNA-seq analysis of 1705 isolated CD45$^+$ cells using the drop-seq method identifies 5 cell clusters in both young (3 months, n = 2) and old (24 months, n = 3) C57BL/6 mice. (C) Stacked bar graph shows the percent of CD45$^+$ cells found in clusters 1-5 in young and old mice from the data defined in panel B. (D) Heatmap of differentially expressed genes that define clusters in panel B. Genetic phenotypes for cell classification are in bold font with asterisk. Genes in common with microglia[25] and peripheral nerve-associated macrophages[18,19] are highlighted in red and blue, respectively. (E) Representative flow cytometric dot plots of F4/80$^+$CD11b$^+$ cells isolated from SI muscularis (MMs), SI mucosal layer (LpMs), and spinal cord (microglia). Numbers on plot are percent of CD45$^+$ cells (mean ± standard deviation). (F) P2ry12 and CD45 expression in LpMs, MMs, and microglia was measured by flow cytometry and is expressed as MFI. (G) Expression of homeostatic microglial genes *P2ry12*, *Trem2*, *Cx3cr1*, *Gpr34*, *Mef2a*, and *Hexb* in sorted LpMs and MMs was measured by qPCR analysis, and results are expressed as relative expression, calculated using the Pfaffl method.[27] Data are mean ± standard error of the mean. *$P < .05$, ***$P < .005$, ****$P < .001$ as determined by one-way analysis of variance with Bonferroni's multiple comparisons (F) and multiple comparisons t-test with post-hoc two-stage linear step-up procedure (G). BioRender.com

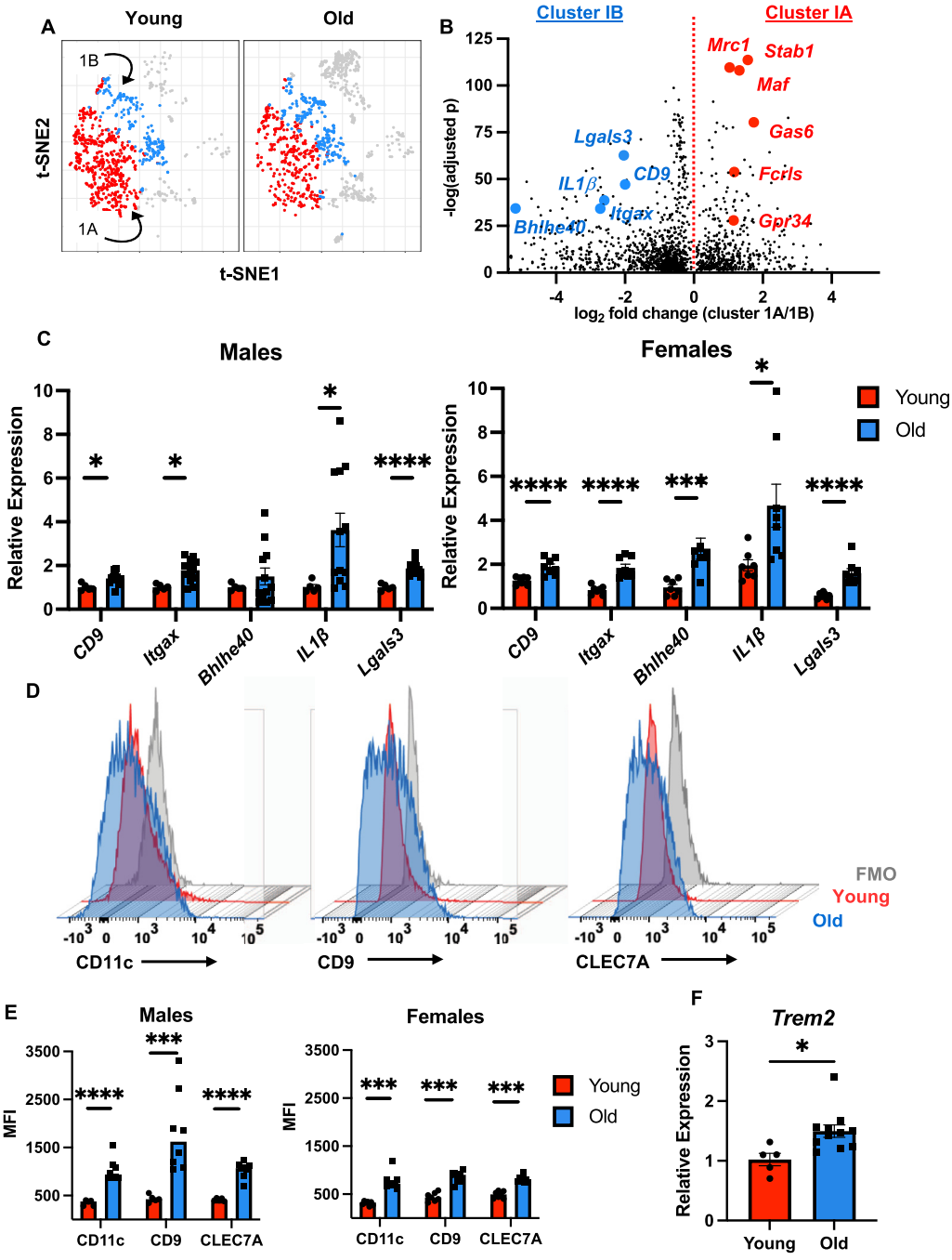

Figure 2. MM expression of DAM-like markers increases with age. (A) t-distrubuted stochastic neighboring embedding (t-SNE) plot of scRNA-seq data for cluster 1 cells (MMs) identifies 2 subclusters (1A and 1B) with subcluster 1A (red) decreasing and subcluster 1B (blue) increasing in old (24 months) compared to young (3 months) mice. (B) Volcano plot shows $\log_2$ fold change of genes in subcluster 1A/1B by significance ($-\log_{10}$ FDR adjusted *P*). DAM[21,22] and homeostatic microglial genes[25] are highlighted in blue and red, respectively. (C) Expression of DAM genes *Cd9*, *Itgax* (CD11c), *Bhlhe40*, *IL1β*, and *Lgals3* by qPCR analysis in sorted MMs ($F4/80^+CD11b^+$ cells) from SI of young (3 months) and old (16–29 months) male and female mice ($n \geq 5$ each). Results are presented as relative expression normalized to young male SI MMs. (D) Representative flow cytometric surface staining of DAM markers CD9, CD11c (*Itgax*), and CLEC7A on MMs from young (red) and old (blue) mice. Gray histograms represent fluorescence minus one (FMO) control. (E) Results from (D) are expressed as MFI for male and female mice. (F) *Trem2* mRNA levels in MMs of male mice measured by qPCR, and results are expressed as relative expression. Data are mean ± standard error of the mean. $^*P < .05$, $^{***}P < .005$, $^{****}P < .001$ by multiple comparisons t-test with post-hoc two-stage linear step-up procedure.

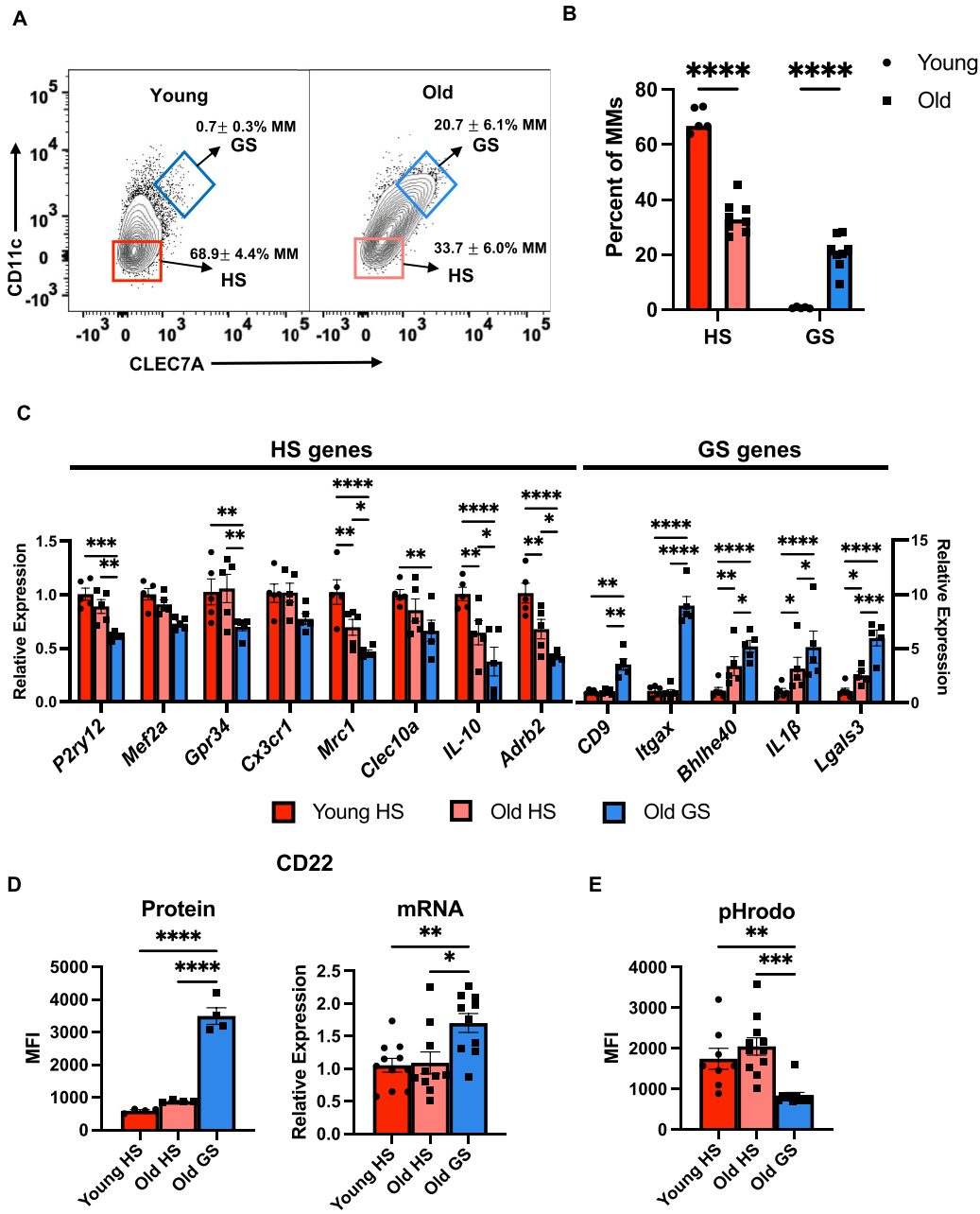

Figure 3. GS MMs have reduced expression of homeostatic microglia and tissue-protective genes. (A) Representative flow cytometric dot plots of F4/80^{+}CD11b^{+} MMs from young and old male mice (n = 5 each) analyzed for CD11c and CLEC7A surface expression demonstrate a CD11c^{-}CLEC7A^{-} homeostatic state (HS) subpopulation present in both young (red box) and old mice (pink box) and a CD11c^{+}CLEC7A^{+} subpopulation (blue boxes) present predominantly in old mice (GS). Numbers on plot represent percent of MMs (mean ± standard deviation). (B) The proportion of HS (CD11c^{-}CLEC7A^{-}) and GS (CD11c^{+}CLEC7A^{+}) MMs in young and old mice expressed as percent of MMs. (C) Sorted GS MMs from old (blue) mice and HS MMs from young (red) and old (pink) mice (n ≥ 5 each, male) were examined for expression of homeostatic state (HS) genes *P2ry12*, *Mef2a*, *Gpr34*, *Cx3cr1*, *Mrc1*, *Clec10a*, *IL10*, and *Adrb2* and GS genes *CD9*, *Itgax*, *Bhlhe40*, *IL1β*, and *Lgals3* by qPCR, and results are shown as relative expression. (D) GS and HS MMs were also examined for CD22 expression by flow cytometry with Alexa Fluor 488-labeled CD22 antibody (protein) and qPCR (mRNA). Results are respectively expressed as MFI and relative expression. (E) HS (CD11c^{-}CLEC7A^{-}) and GS (CD11c^{+}CLEC7A^{+}) colon MMs were assessed for green fluorescence 1 hour after pHrodo Green Zymosan Bioparticles were injected into the colon muscularis of young (2 months) and old (22 months) mice (n ≥ 8 each, male). Results are expressed as MFI of the phagocytic (pHrodo^{+}) MMs. Data are mean ± standard error of the mean. *$P < .05$, **$P < .01$, ***$P < .005$, ****$P < .001$ by two-way analysis of variance with Bonferroni's multiple comparisons (B) or with post-hoc two-stage linear step-up procedure (C) and one-way analysis of variance with Bonferroni's multiple comparisons (D, E).

A volcano plot analysis (Figure A2B) indicated that the subcluster 1A was enriched for tissue-protective/homeostatic microglial genes relative to subcluster 1B, including *Mrc1* (CD206), *Stab1*, *Maf*, *Gas6*, *Fcrls*, and *Gpr34*.[21,25] By contrast, the subcluster 1B was enriched for several DAM markers, including *Cd9*, *Itgax* (CD11c), *Lgals3*, *Bhlhe40*, and *IL-1β*.[21,22] To confirm that this finding was not exclusive to male mice, SI MMs ($CD45^+F4/80^+CD11b^+$ cells) sorted from young and old mice of both sexes were examined for the expression of DAM markers including *CD9*, *Itgax*, *Bhlhe40*, *IL-1β*, and *Lgals3.* Expression of several of these DAM markers was markedly higher in old mice MMs than in young mice MMs including *Cd9*, *Itgax* (CD11c), *IL-1β*, and *Lgals3*, which reached statistical significance in both males and females, and *Bhlhe40* in females (Figure 2C). MMs ($CD45^+F4/80^+CD11b^+$ cells) were also examined for surface expression of DAM markers CD9, CD11c, and CLEC7A. A significantly higher expression of all 3 markers was detected in old mice than in young mice in both sexes by MFI (Figure 2D and E). To evaluate the kinetics of DAM gene upregulation as a function of age, MMs from young (3 months), mid-aged (10 months), and old (24 months) male mice were examined for the expression of CD9, CD11c, and CLEC7A. These genes increased in an age-dependent manner, with lowest levels seen at 3 months of age ($P < .001$) (Figure A2B). Expression of the innate immunity receptor *Trem2* was also higher ($P < .01$) in MMs from old mice than in those from young mice (Figure 2F), consistent with its known upregulation in microglia collected from mice with advanced age or a neurodegenerative disease.[21,22] Similar to microglia,[21] the kinetics of *Trem2* elevation occurred at a later age compared to CD9, CD11c, and CLEC7A, with increased expression observed in 24-month-old mice but not in 10-month-old mice (Figure A2C). Collectively, the data indicate that old mice have an MM subpopulation with properties like those of DAM microglia.

The Geriatric MM Subpopulation Defined by CD11c and Clec7A Expression Have Reduced Expression of Homeostatic Genes and Phagocytic Activity

Flow cytometry studies confirmed that old mice have a $CD11c^+CLEC7A^+$ MM subpopulation (GS MMs) that is almost absent in young mice (Figure 3A and B). The rise in GS MMs corresponded to a decline in $CD11c^-CLEC7A^-$ (homeostatic state [HS]) MMs in old mice. To better understand the potential functional significance of this GS subpopulation, MMs from young (3 months) and old (22 months) mice ($n \geq 5$/group) were sorted based on the differential surface expression of CD11c and CLEC7A. qPCR Analysis comparing the $CD11c^+CLEC7A^+$ (GS) MMs to the $CD11c^-CLEC7A^-$ (HS) MMs from both young and old mice indicated that GS MMs express significantly lower levels of homeostatic microglial genes,[25] including *P2ry12*, *Mef2a, Gpr34*, and *Cx3cr1*, and tissue-protective genes,[15,34] including *Mrc1*, *Clec10a*, and *IL10*, and higher levels of the DAM genes *CD9*, *Itgax*, *Bhlhe40*, *IL1β*, and *Lgals3* than HS MMs (Figure 3C). Sympathetic neurons regulate the MM homeostatic function via signaling through the β2-adrenergic receptor.[1,6,7] GS MMs also had lower gene expression of the β2-adrenergic receptor (*Adrb2*) than HS MMs (Figure 3C), suggesting that GS MMs have diminished responsiveness to extrinsic signals.

Compared to HS MMs from young and old mice, GS MMs exhibited significantly higher protein and mRNA expression of CD22, a canonical B-cell receptor (Figure 3D). Increased CD22 expression in the microglia of geriatric mice results in impairment of their homeostatic phagocytic function.[35] To evaluate the phagocytic activity of MMs, pH-sensitive beads (pHrodo-labeled Zymosan Bioparticles) were injected into the colons of young (2 months) and old (22 months) mice ($n \geq 8$/group). One hour after injections, the tissue was harvested, and flow cytometry was performed to assess the pHrodo signal in MMs. Although the percent of phagocytic ($pHrodo^+$) MMs did not significantly differ between young and old mice (Figure A3A and B), the fluorescence intensity of phagocytic MMs was significantly reduced for GS compared with that of HS MMs (Figure 3E), indicating diminished phagocytic activity in GS MMs. Collectively, the data suggest that age-dependent acquisition of the GS phenotype drives neuroinflammation and results in the loss of MM function important for ENS homeostasis.

GS Phenotype is Associated With Intracellular α-SYN and Clearance of Apoptotic Neurons

Having observed that the GS MM phenotype is defined by the expression of DAM markers, we next asked whether its acquisition might involve the clearance of neuronal debris and apoptotic neurons as previously described for microglia DAM marker development.[22,36] Aggregates of α-SYN, a protein involved in neuronal synaptic vesicle trafficking,[37,38] accumulate in dystrophic enteric neurons of geriatric rats.[39,40] MMs surrounding these dystrophic neurons have been observed to contain α-SYN aggregates.[39] Two series of experiments were done to explore whether clearance of α-SYN neuronal debris may be involved in the GS phenotype. First, whole-mount sections of the SI muscularis tissue from young (3 months) and old (24 months) mice ($n \geq 4$/group) were stained with antibodies to α-SYN together with antibodies to major histocompatibility complex class II (MMs) and Hu (neurons) (Figure 4A). In a second set of experiments, the dissociated cells from the muscularis tissue were subjected to intracellular staining with Alexa Fluor 488-conjugated α-SYN antibodies, and the percent of $α\text{-SYN}^+$ MMs was assessed by flow cytometry (Figure 4B). In both experiments, the percent of $α\text{-SYN}^+$ MMs was significantly higher ($P < .005$) in old mice than in young mice (Figure 4A and B). Backgating onto total MMs indicated that the $α\text{-SYN}^+$ MMs were enriched for coexpression of the GS markers CD11c and CLEC7A (Figure 4C). Also, the α-SYN MFI was significantly higher ($P < .001$) in GS MMs than in HS MMs from young and old mice (Figure 4D). Because aging is associated with elevated numbers of apoptotic neurons in the

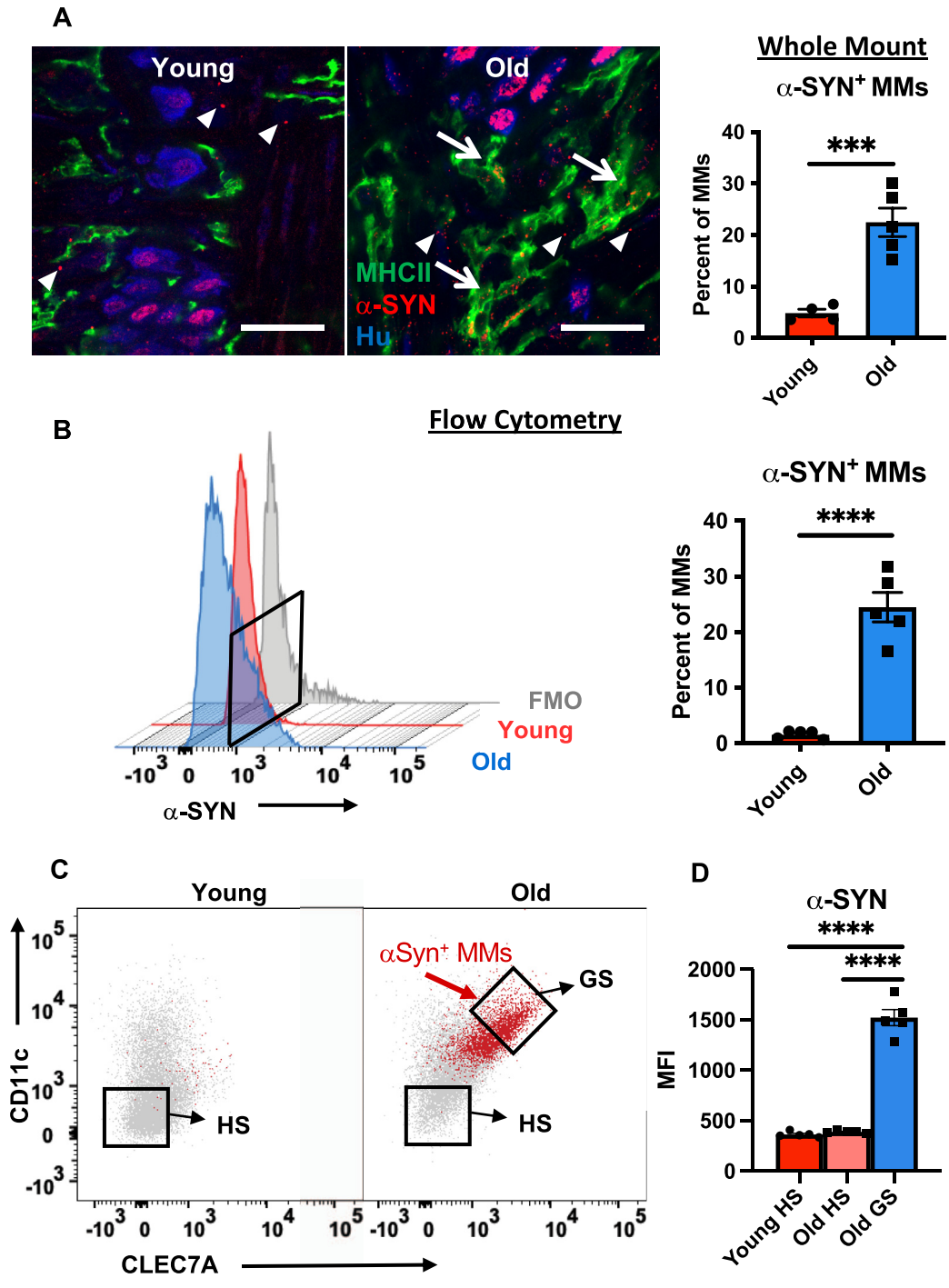

Figure 4. MMs acquire the GS phenotype through clearance of α-SYN neuronal debris. (A) SI muscularis tissue from young (3 months) and old (23–28 months) mice (n ≥ 4 each) were stained with antibodies to α-SYN (red), Hu (pan-neuronal marker, blue), and major histocompatibility complex class II (macrophage marker, green), and a minimum of 8 randomly selected fields containing myenteric ganglia were examined by confocal microscopy. α-SYN aggregates (arrowheads) and MMs containing α-SYN (arrows) are shown. The percentage of α-SYN$^+$ MMs was significantly higher in old mice than in young mice. (B) Representative flow cytometric histograms of intracellular immunofluorescent staining of MMs with Alexa Fluor 488-labeled α-SYN antibody in old and young mice (n = 6 each). FMO (grey histogram) was used to determine the cutoff (black box) for defining α-SYN$^+$ MMs, and results are expressed as percentage of α-SYN$^+$ MMs. (C) When backgated onto MMs (grey), α-SYN$^+$ MMs (red) were enriched for cells coexpressing GS markers CD11c and CLEC7A (representative image of 2 independent experiments). (D) The α-SYN levels expressed as MFI in GS (CD11c$^+$CLEC7A$^+$) and HS (CD11c$^-$CLEC7A$^-$) MMs. Data are mean ± standard error of the mean. ***$P < .005$ by t-test (A and B) and one-way analysis of variance with Bonferroni's multiple comparisons test (D). Scale bars 25 μm (**** $P < .001$).

myenteric plexus of mice,[15] we examined whether macrophage clearance of apoptotic neurons is a function associated with the geriatric phenotype. Bone marrow-derived macrophages were cocultured with ultraviolet-irradiated fluorescent enteric neurons (apoptotic; aNeurons) and examined for intracellular fluorescence and expression of GS markers (CD11c and Clec7A). Macrophages that had phagocytosed aNeurons were significantly enriched ($P < .05$) for CD11c and CLEC7A expression (Figure A4). Collectively the data indicate that the GS phenotype ($CD11c^+CLEC7A^+$) is associated with intracellular accumulation of α-SYN and clearance of apoptotic neurons.

Human MMs Exhibit Age-Dependent Acquisition of the GS Phenotype

Changes in the immune composition of human colon muscularis with age have been poorly explored. Surgical colon specimens were collected from 26 patients whose age ranged from 25 to 95 years [median = 70.5, interquartile range = 32.25 (52.25-84.5)]. Nineteen of the 26 patients (73.1%) were female, and indications for surgery are listed in Table 1. After dissecting the muscle layer and enzymatically digesting the tissue, flow cytometry was performed to assess levels of total leukocytes ($CD45^+$), MMs ($CD45^+CD14^+CD3^-CD19^-$), lymphocytes ($CD45^+CD14^-CD3^+CD19^+$), and dendritic cells (DCs) ($CD45^+CD14^-CD11c^+$) (Figure A5A and B). Age was associated with a modest increase in leukocytes (expressed as percentage of live cells), but the correlation was not significant (Figure A5B). Measured as a percent of $CD45^+$ cells, MMs increased ($R^2 = 0.05$, $P = .28$), and lymphocytes declined ($R^2 = 0.05$, $P = .27$) with age while DCs remained stable (Figure A5C). Human MMs consist of several distinct subpopulations defined by unique genetic expression profiles.[33] To help define macrophage subpopulations, MMs ($CD14^+$ cells) were also assessed for surface expression of monocyte/macrophage markers CD11b and CD64. Three MM subpopulations were identified, MM_1 ($CD11b^+CD14^{high}CD64^+$), MM_2 ($CD11b^+CD14^{high}CD64^-$), and MM_3 ($CD11b^+CD14^{int}$) (Figure 5A). Age was associated with an increase in the MM_1 subpopulation ($R^2 = 0.13$, $P = .06$) and decline in the others (Figure 5B). Expression of known MM markers CD206 (*MRC1*) and *ADRB2*[1,6,15] (Figure 5C) and homeostatic microglial genes, including *P2RY12*, *TREM2*, *CX3CR1*, *GPR34*, and *C1QC* (Figure 5D), was higher in the MM_1 subpopulation than that in MM_2 and MM_3 subpopulations, suggesting that MM_1 macrophages represent a NAM subpopulation analogous to murine MMs (Figure 1). Next, we examined whether age was associated with a geriatric MM phenotype like that observed in mice (Figures 2 and 3). Immunostaining of colon tissue sections with antibodies to CD14 and the GS marker CLEC7A (Dectin-1) demonstrated colabeling of MMs (Figure 5E). Flow cytometry revealed a statistically significant correlation between increasing CLEC7A surface expression and age ($R^2 = 0.15$, $P = .046$) in the MM_1 subpopulation but not in the MM_2 or MM_3 subpopulations (Figure 5F). Within the MM_1 subpopulation, GS ($CD11c^+CLEC7A^+$) and HS ($CD11c^-CLEC7A^-$) MMs were identified (Figure 5G), and the proportion of GS MMs rose ($R^2 = 0.16$, $P = .10$) and that of HS MMs declined ($R^2 = 0.18$, $P = .07$) as a function of age (Figure 5G). A qPCR analysis of the sorted MM subpopulations revealed an age-dependent increase in other GS genes including *IL1B* ($R^2 = 0.08$, $P = .2$) (Figure 5H), *TREM2* ($P = .002$) (Figure 5I), *ITGAX* ($R^2 = 0.05$, $P = .31$) (Figure A5D), and *CD22* ($P = .01$) (Figure A5E) exclusive to the MM_1 subpopulation. Collectively, the data indicate that aging results in an expansion of human MMs, particularly the MM_1 subpopulation, which has a genetic signature common with NAMs, and this subpopulation acquires a geriatric phenotype similar to that of mice.

α-SYN MM Accumulation is Associated With the GS Phenotype in Humans

An age-dependent increase in α-SYN deposition has been observed in the human ENS[41]; however, whether it accumulates in MMs and alters their phenotype is unknown. Colon tissue sections were incubated with antibodies to α-SYN, PGP9.5 (neurons) and CD14 (macrophages). Abundant α-SYN was detected in enteric neurons within the myenteric plexus (Figure 6A) and colocalized to $CD14^+$ MMs (arrows) bordering the enteric ganglia (Figure 6B). Intracellular staining with Alexa Fluor 488-conjugated α-SYN antibodies was performed on dissociated colonic muscularis tissue, and the α-SYN signal in the MM subpopulations was assessed by flow cytometry (Figure 6C). Higher α-SYN levels were found in MM_1 than in MM_2 and MM_3 macrophages, consistent with MM_1 macrophages serving a role in clearance of neuronal debris (Figure 6C). Importantly, GS ($CD11c^+CLEC7A^+$) MM_1 macrophages demonstrated a significantly higher α-SYN signal than HS ($CD11c^-CLEC7A^-$) MM_1 macrophages (Figure 6D). Backgating onto total MM_1 macrophages indicated that MMs with high levels of α-SYN ($\alpha\text{-SYN}^{Hi}$ MM_1) (Figure 6D) were enriched for coexpression of the GS markers CD11c and CLEC7A (Figure 6E). Collectively, the data suggest that the increasing intracellular accumulation of α-SYN causes MM_1 macrophages to acquire a geriatric phenotype.

Discussion

The salient feature of the data presented in this report is the finding of an age-dependent MM genetic signature in a subset of macrophages that mirrors the microglia DAM phenotype. This geriatric phenotype, observed in both mice and humans, is associated with intracellular accumulation of α-SYN and characterized by loss of homeostatic function and increased inflammatory activation. The following comments are pertinent with respect to these findings.

Enteric neurons are vulnerable to age-related degeneration and play an important role in GI dysfunction in elderly individuals.[15,42] However, the role of ENS immune cells in the gut dysfunction seen in the elderly is unknown. Our studies were designed to address this question. Using single-cell transcriptomics of $CD45^+$ cells from the SI

muscularis, we identified 5 distinct immune cell clusters that respectively represent MMs, T cells, immature and mature B cells, and an unassigned population. We did not identify mast cells or DCs previously seen at low levels in the gut muscularis[15,43] and do not exclude the possibility that our clusters contain low numbers of other unidentified cell types.

Our studies focused on the MM cell population (cluster 1) because MM functional alterations have been previously implicated in gut dysmotility.[1–6,8–15] Specifically, we asked whether MMs regulate age-dependent gut dysfunction through properties similar to those used by microglia in neurodegenerative processes. Indeed, microglia express "sensome" genes that include pattern-recognition receptors, Fc receptors, chemokine and cytokine receptors, purinergic receptors, and receptors involved in cell adhesion[44] and are tailored for their specialized support role in the central nervous system.[20] While some components of this sensing apparatus are shared among all macrophages, including Toll-like and Fc receptors,[45] many of them are unique or highly enriched in microglia and peripheral NAMs.[18,19,25] Among these are P2ry12, C1q, Gpr34, Csf1r, and Cx3cr1, which are involved in microglia housekeeping and neuroprotection.[25,46–49] For example, microglia directly sense neuronal mitochondrial activity through the purinergic receptor P2ry12, enabling a rapid neuroprotective response to neuronal injuries.[46] Gpr34, another member of the P2ry12

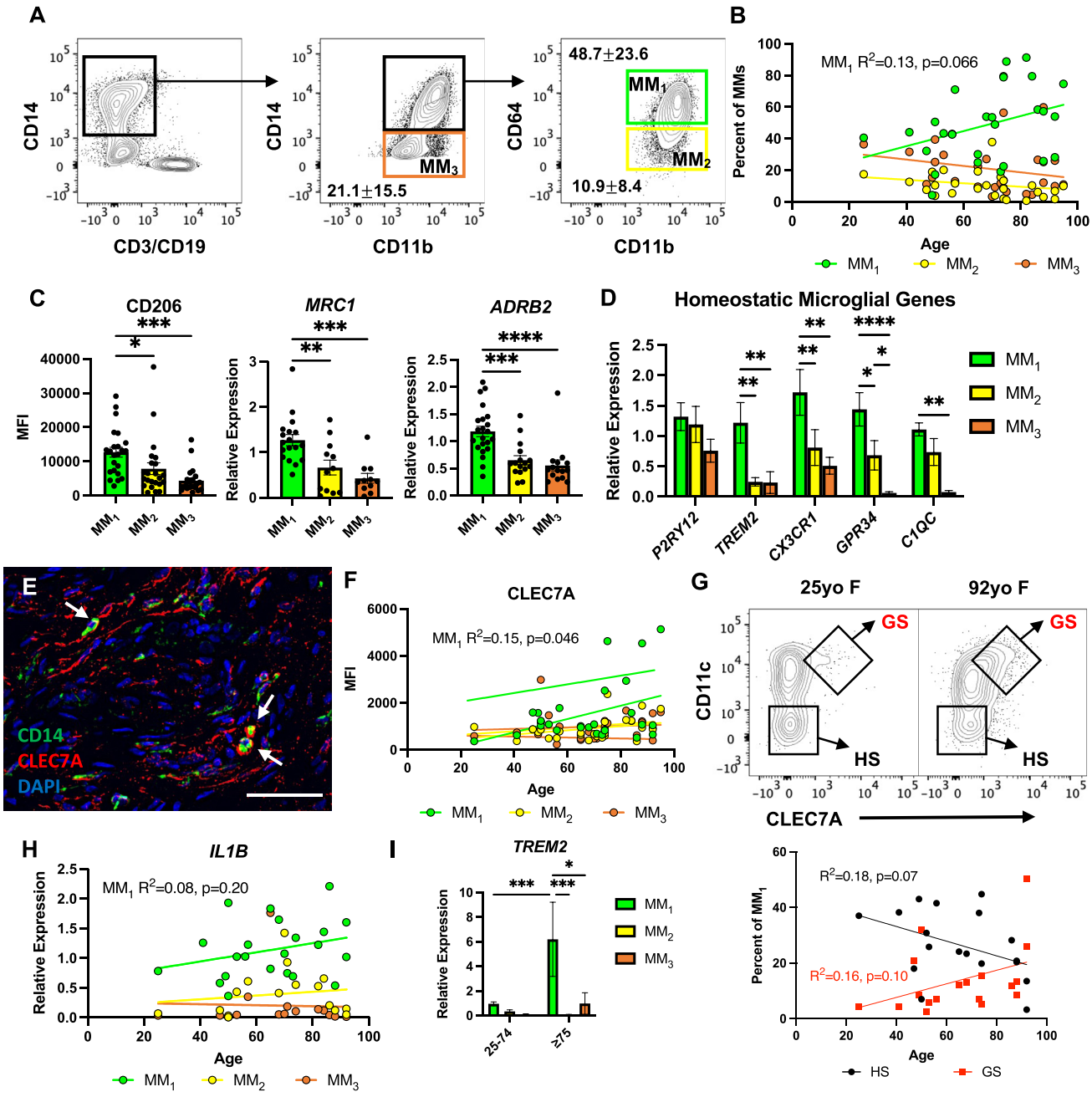

receptor family, and C1q, a component of the complement system, regulate the microglial phagocytic function and removal of neuronal debris.[47,48,50] Also, through the Cx3cr1 receptor, microglia sense the neuronally expressed chemokine fractalkine to regulate synaptic pruning.[49]

We found that MMs, similar to other peripheral NAMs,[18,19] express several microglial homeostatic genes including *P2ry12*, *C1q*, and *Gpr34*, as well as *Csf1r* and *Cx3cr1*,[2,14] suggesting they function to sense environmental perturbations and provide housekeeping support to the ENS, as is the case for microglia. Supporting the important role these genes have in ENS homeostasis, macrophage-specific deletion of *C1qa* results in changes in the enteric neuron gene expression and altered intestinal motility.[51] We found the microglial genetic signature in MMs of both mice and humans, males and females, and in SI and colon. Interestingly, many of the microglial homeostatic genes showed higher expression in female mice than in male mice (Figure A1E). Whether similar sex differences exist in humans and if these differences have functional consequences are the subject of ongoing investigation.

Comparison of old to young mice indicated that MMs express similar levels of homeostatic microglial genes, but expression of GS genes, which mirror the microglial DAM phenotype, is acquired with aging. In microglia, the DAM phenotype is believed to represent the compensatory upregulation of a neurodegeneration-associated molecular pattern apparatus, which initially has a protective role that increases neuronal debris clearing but eventually drives neuroinflammation.[52] While it remains unclear whether the GS phenotype has a protective role at an early stage, we found that the MM GS phenotype is associated with increased expression of the proinflammatory cytokine IL-1β (Figures 2B and 3C) and reduced expression of the anti-inflammatory cytokine IL-10 (Figure 3C). GS MMs also exhibited increased CD22 expression that, similar to microglia,[35] resulted in the loss of phagocytic activity (Figure 3E). GS MMs also had reduced expression of Adrb2 (Figure 3C), the adrenergic receptor important for MM-mediated ENS recovery following enteric infections.[1,6,7] This offers a potential explanation for why elderly individuals have diminished resilience to enteric infections such as that by *Clostridioides difficile*.[53] Collectively, our data suggest that the GS phenotype has a deleterious effect on ENS homeostasis by promoting neuroinflammation and accumulation of degenerative debris.[15]

Consistent with previous findings that phagocytosis of neuronal debris promotes the microglial DAM phenotype,[22,36] we found that GS, but not HS, macrophages contain high levels of α-SYN aggregates, suggesting that phagocytosis of neuronal debris also promotes acquisition of the GS phenotype. Our findings may have relevance to the pathogenesis of neurodegenerative disorders in the gut. α-SYN aggregation, the hallmark pathogenic factor in Parkinson's disease (PD), is found in the gut of PD patients, and emerging evidence suggests the disease initiates in the gut and is transferred centrally through the vagal pathway.[54] Elevation in enteric α-SYN is associated with increased gut inflammation and delayed intestinal transit in PD patients and animal models.[55,56] We propose that PD and other neurodegenerative disorders accelerate the accumulation of GS macrophages, thereby causing ENS neuroinflammation and disruption of gut function. Additionally, the loss of HS MMs could also contribute to disease pathogenesis. Homeostatic microglia play a role in clearing α-SYN aggregates via autophagy.[57] Therefore, declining numbers of HS MMs in old mice could explain why in a PD animal model, after α-SYN gut injections, brain transmission was observed in old but not young mice.[55] Further clarification of the role of gut macrophages in PD

Figure 5. Human MMs have a NAM genetic signature and acquire a geriatric phenotype with age. (A) Representative flow cytometric dot plots demonstrating the gating scheme for human MMs. $CD45^+$ cells isolated from the muscularis layer of human colon were examined for surface expression of monocyte/macrophage markers CD14, CD11b, and CD64. Three subpopulations of MMs were identified based on the intensity of marker expression: MM_1 ($CD11b^+CD14^{high}CD64^+$, green), MM_2 ($CD11b^+CD14^{high}CD64^-$, yellow), and MM_3 ($CD11b^+CD14^{Int}$, orange). Numbers on plot are percentage of $CD14^+$ cells (mean $\pm$ standard deviation). (B) The relationship between proportions of MM subpopulations (expressed as percentage of total MMs [$CD14^+$]) and age in years. Regression lines and Pearson correlation statistics (for MM_1) are shown. (C) MM subpopulations were examined for CD206 (*MRC1*) and *ADRB2* expression by flow cytometry and qPCR. Results are expressed as MFI and relative expression. (D) Expression of microglial homeostatic genes *P2RY12*, *TREM2*, *CX3CR1*, *GPR34*, and *C1QC* by qPCR analysis in MM subpopulations. Results are presented as relative expression normalized to MM_1 macrophages. (E) Colon tissue section (80-year-old female [80yo F]) stained with antibodies to CLEC7A (red) and CD14 (macrophage marker, green) and 4',6-diamidino-2-phenylindole (DAPI, blue) was examined by a Keyence Fluorescence Microscope. MMs expressing *CLEC7A* are shown (arrows). (F) The relationship between the surface expression of CLEC7A in MM subpopulations as measured by flow cytometry (expressed as MFI) and age (in years). Regression lines and Pearson correlation statistics (for MM_1) are shown. (G) Representative flow cytometric dot plots of MM_1 macrophages from a young (25-year-old female [25yo F]) and old (92-year-old female [92yo F]) patient analyzed for CD11c and CLEC7A surface expression with gates defining HS ($CD11c^-CLEC7A^-$) and GS ($CD11c^+CLEC7A^+$) MM_1. The relationship between proportions of GS/HS MM_1 subpopulations (expressed as percentage of total MM_1) and age in years. Regression lines and Pearson correlation statistics are shown. (H) The relationship between *IL1B* expression in sorted MM subpopulations as measured by qPCR and age (in years). Regression lines and Pearson correlation statistics (for MM_1) are shown. (I) Expression of *TREM2* in MM subpopulations by qPCR analysis from patients aged 25–74 years and $\geq$75 years. Data are given as mean $\pm$ standard error of the mean. $^*P < .05$, $^{**}P < .01$, $^{***}P < .005$, $^{****}P < .001$ by one-way analysis of variance with Bonferroni's multiple comparisons test (C), two-way analysis of variance with post-hoc two-stage linear step-up (D), or Bonferroni's multiple comparisons test (I). Scale bar 50 μm.

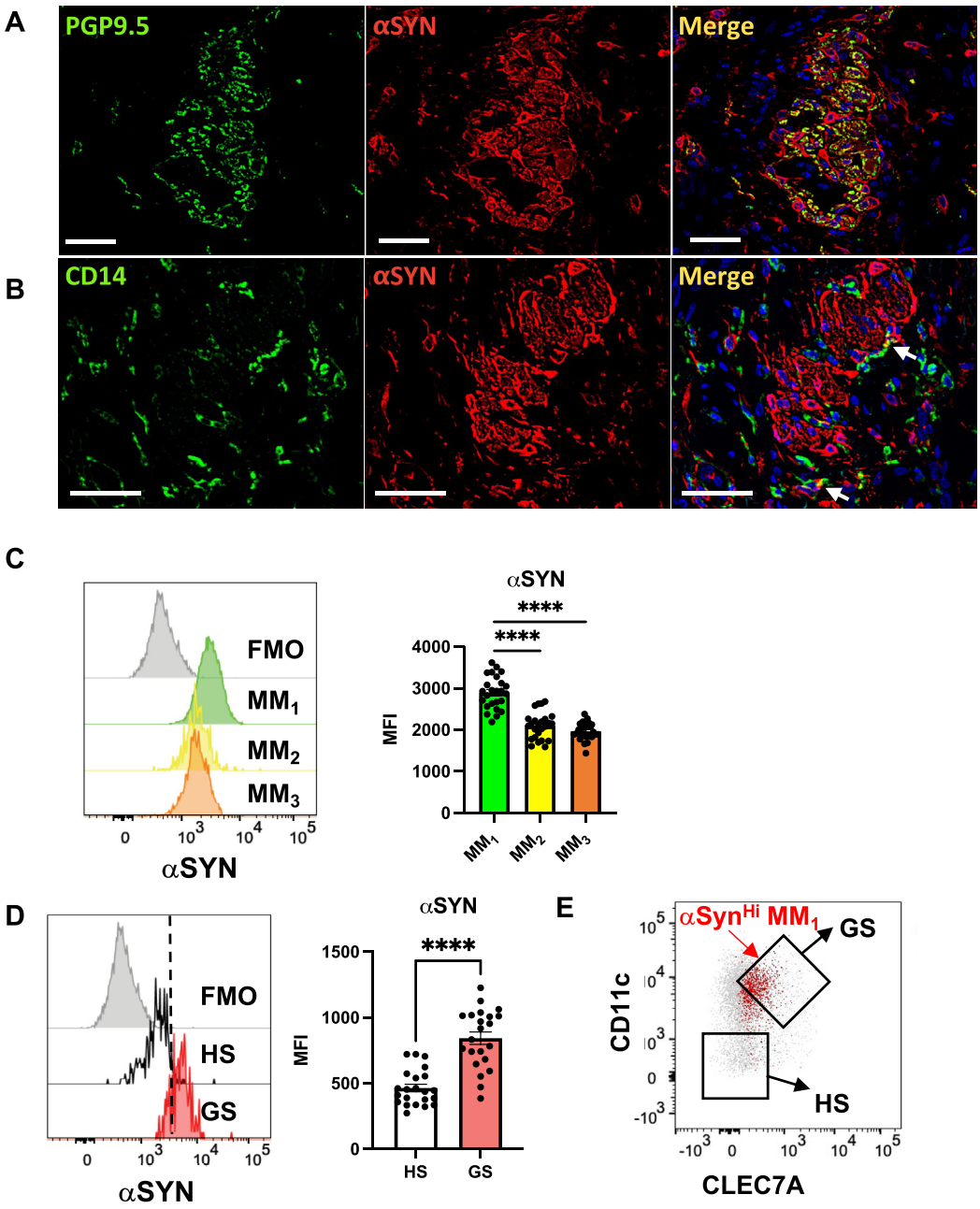

Figure 6. α-SYN accumulation in human MMs associated with geriatric phenotype. (A) Colon tissue section (82-year-old female) stained with antibodies to PGP9.5 (neuron marker, green) and α-SYN (red) and 4',6-diamidino-2-phenylindole (DAPI) (blue) examined by a Keyence Fluorescence Microscope. (B) Colon tissue section (84-year-old male) stained with antibodies to CD14 (macrophage marker, green) and α-SYN (red) and DAPI (blue). Colocalization of α-SYN with MMs are shown (arrows). (C) Representative flow cytometric histograms of intracellular immunofluorescent staining of α-SYN in MM subpopulations (grey histogram is FMO). The α-SYN levels in MM_1, MM_2, and MM_3 macrophages are expressed as MFI. (D) Representative flow cytometric histograms of α-SYN signal in HS ($CD11c^-CLEC7A^-$, white) and GS ($CD11c^+CLEC7A^+$, red) MM_1 macrophages (grey histogram is FMO). The dotted black line is the cutoff for defining α-SYN^{Hi} MMs. The α-SYN levels in HS and GS MM_1 macrophages are expressed as MFI. (E) When backgated onto total MM_1 (grey), α-SYN^{Hi} MM_1 macrophages (red) were enriched for cells coexpressing GS markers CD11c and CLEC7A. Data are given as mean $\pm$ standard error of the mean. ****$P < .001$ by t-test (D). Scale bars 50 μm. DAPI, 4',6-diamidino-2-phenylindole.

and other neurodegenerative disorders is necessary to determine whether targeting the GS immunophenotype may be effective in treating these disorders.

We conclude that human MMs acquire a GS phenotype similar to that of mice based on higher proportions of $CD11c^+CLEC7A^+$ MM_1 macrophages (Figure 5G) and

increased expression of *Trem2* and *CD22* with age (Figure 5I, Figure A4E). However, our findings in humans and mice were not entirely equivalent. Correlations between age and GS gene expression did not reach statistical significance for *IL1B* ($R^2 = 0.08$, $P = .2$) (Figure 5H) or *ITGAX* ($R^2 = 0.05$, $P = .31$) (Figure A5D). A potential explanation is the heterogeneity of our human samples which differed based on surgical indications. Notably, exclusion of the 2 specimens with the highest leukocyte infiltration (corresponding to patients with adhesive mesh and perforated diverticulitis [Figure A4B]) resulted in a better correlation between *IL1B* expression and age ($P = .07$). This suggests that certain inflammatory conditions may mask the effects of age. Additional limitations to our study include low numbers of young patients (only 1 patient <40 years of age) and male subjects (7/26). Future studies involving greater numbers of patients and functional measures of gut motility are necessary to determine whether the GS phenotype may serve as a biomarker or therapeutic target for age-related GI disorders.

Conclusion

In conclusion, our studies document, for the first time, that MMs function as the ENS microglia, serving an important housekeeping and neuroprotective role. They share a common genetic signature with microglia and peripheral NAMs, which enables environmental sensing and communication with enteric neurons, and acquire a GS phenotype with aging that reduces their functional efficacy, resulting in neuroinflammation and disruption of gut motility.

Supplementary Materials

Material associated with this article can be found in the online version at https://doi.org/10.1016/j.gastha.2022.09.006.

References

1. Gabanyi I, Muller PA, Feighery L, et al. Neuro-immune interactions drive tissue programming in intestinal macrophages. Cell 2016;164:378–391.
2. Muller PA, Koscso B, Rajani GM, et al. Crosstalk between muscularis macrophages and enteric neurons regulates gastrointestinal motility. Cell 2014;158:300–313.
3. Luo J, Qian A, Oetjen LK, et al. TRPV4 channel signaling in macrophages promotes gastrointestinal motility via direct effects on smooth muscle cells. Immunity 2018;49:107–119.e4.
4. Becker L, Spear ET, Sinha SR, et al. Age-related changes in gut microbiota alter phenotype of muscularis macrophages and Disrupt gastrointestinal motility. Cell Mol Gastroenterol Hepatol 2019;7:243–245.e2.
5. Ji S, Traini C, Mischopoulou M, et al. Muscularis macrophages establish cell-to-cell contacts with telocytes/PDGFRα-positive cells and smooth muscle cells in the human and mouse gastrointestinal tract. Neurogastroenterol Motil 2020;33:e13993.
6. Matheis F, Muller PA, Graves CL, et al. Adrenergic signaling in muscularis macrophages Limits infection-induced neuronal loss. Cell 2020;180:64–78.e16.
7. Ahrends T, Aydin B, Matheis F, et al. Enteric pathogens induce tissue tolerance and prevent neuronal loss from subsequent infections. Cell 2021;184:5715–5727.e12.
8. Matteoli G, Gomez-Pinilla PJ, Nemethova A, et al. A distinct vagal anti-inflammatory pathway modulates intestinal muscularis resident macrophages independent of the spleen. Gut 2014;63:938–948.
9. Choi KM, Kashyap PC, Dutta N, et al. CD206-positive M2 macrophages that express heme oxygenase-1 protect against diabetic gastroparesis in mice. Gastroenterology 2010;138:2399–2409, 2409 e1.
10. Grover M, Bernard CE, Pasricha PJ, et al. Diabetic and idiopathic gastroparesis is associated with loss of CD206-positive macrophages in the gastric antrum. Neurogastroenterol Motil 2017;29:1–8.
11. Wehner S, Behrendt FF, Lyutenski BN, et al. Inhibition of macrophage function prevents intestinal inflammation and postoperative ileus in rodents. Gut 2007;56:176–185.
12. Cipriani G, Gibbons SJ, Miller KE, et al. Change in populations of macrophages promotes development of delayed gastric emptying in mice. Gastroenterology 2018;154:2122–2136.e12.
13. Cipriani G, Gibbons SJ, Verhulst PJ, et al. Diabetic Csf1op/op mice lacking macrophages are protected against the development of delayed gastric emptying. Cell Mol Gastroenterol Hepatol 2016;2:40–47.
14. De Schepper S, Verheijden S, Aguilera-Lizarraga J, et al. Self-maintaining gut macrophages are Essential for intestinal homeostasis. Cell 2018;175:400–415.e13.
15. Becker L, Nguyen L, Gill J, et al. Age-dependent shift in macrophage polarisation causes inflammation-mediated degeneration of enteric nervous system. Gut 2018;67:827–836.
16. Kolter J, Feuerstein R, Zeis P, et al. A subset of skin macrophages contributes to the surveillance and Regeneration of local nerves. Immunity 2019;50:1482–1497.e7.
17. Ural BB, Yeung ST, Damani-Yokota P, et al. Identification of a nerve-associated, lung-resident interstitial macrophage subset with distinct localization and immunoregulatory properties. Sci Immunol 2020;5:eaax8756.
18. Wang PL, Yim AKY, Kim KW, et al. Peripheral nerve resident macrophages share tissue-specific programming and features of activated microglia. Nat Commun 2020;11:2552.
19. Ydens E, Amann L, Asselbergh B, et al. Profiling peripheral nerve macrophages reveals two macrophage subsets with distinct localization, transcriptome and response to injury. Nat Neurosci 2020;23:676–689.
20. Hickman S, Izzy S, Sen P, et al. Microglia in neurodegeneration. Nat Neurosci 2018;21:1359–1369.

21. Keren-Shaul H, Spinrad A, Weiner A, et al. A unique microglia type associated with restricting development of Alzheimer's disease. Cell 2017;169:1276–1290.e17.
22. Krasemann S, Madore C, Cialic R, et al. The TREM2-APOE pathway drives the transcriptional phenotype of dysfunctional microglia in neurodegenerative diseases. Immunity 2017;47:566–581.e9.
23. Mathys H, Adaikkan C, Gao F, et al. Temporal tracking of microglia activation in neurodegeneration at single-cell resolution. Cell Rep 2017;21:366–380.
24. Mrdjen D, Pavlovic A, Hartmann FJ, et al. High-dimensional single-cell mapping of central nervous system immune cells reveals distinct myeloid subsets in health, aging, and disease. Immunity 2018;48:380–395.e6.
25. Butovsky O, Jedrychowski MP, Moore CS, et al. Identification of a unique TGF-beta-dependent molecular and functional signature in microglia. Nat Neurosci 2014;17:131–143.
26. Manglani M, Gossa S, McGavern DB. Leukocyte isolation from brain, spinal cord, and meninges for flow cytometric analysis. Curr Protoc Immunol 2018;121:e44.
27. Pfaffl MW. A new mathematical model for relative quantification in real-time RT-PCR. Nucleic Acids Res 2001;29:e45.
28. Stuart T, Butler A, Hoffman P, et al. Comprehensive integration of single-cell data. Cell 2019;177:1888–1902.e21.
29. Benjamini Y, Hochberg Y. Controlling the false discovery rate: a practical and powerful approach to multiple testing. J R Stat Soc Ser B (Methodological) 1995;57:289–300.
30. Buttgereit A, Lelios I, Yu X, et al. Sall1 is a transcriptional regulator defining microglia identity and function. Nat Immunol 2016;17:1397–1406.
31. Sedgwick JD, Schwender S, Imrich H, et al. Isolation and direct characterization of resident microglial cells from the normal and inflamed central nervous system. Proc Natl Acad Sci U S A 1991;88:7438–7442.
32. Verheijden S, De Schepper S, Boeckxstaens GE. Neuron-macrophage crosstalk in the intestine: a "microglia" perspective. Front Cell Neurosci 2015;9:403.
33. Domanska D, Majid U, Karlsen VT, et al. Single-cell transcriptomic analysis of human colonic macrophages reveals niche-specific subsets. J Exp Med 2022;219:e20211846.
34. Gordon S. Alternative activation of macrophages. Nat Rev Immunol 2003;3:23–35.
35. Pluvinage JV, Haney MS, Smith BAH, et al. CD22 blockade restores homeostatic microglial phagocytosis in ageing brains. Nature 2019;568:187–192.
36. Heneka MT, Kummer MP, Stutz A, et al. NLRP3 is activated in Alzheimer's disease and contributes to pathology in APP/PS1 mice. Nature 2013;493:674–678.
37. Sun J, Wang L, Bao H, et al. Functional cooperation of α-synuclein and VAMP2 in synaptic vesicle recycling. Proc Natl Acad Sci U S A 2019;116:11113–11115.
38. Vargas KJ, Makani S, Davis T, et al. Synucleins regulate the kinetics of synaptic vesicle Endocytosis. J Neurosci 2014;34:9364–9376.
39. Phillips RJ, Billingsley CN, Powley TL. Macrophages are unsuccessful in clearing aggregated alpha-synuclein from the gastrointestinal tract of healthy aged Fischer 344 rats. Anat Rec (Hoboken) 2013;296:654–669.
40. Phillips RJ, Walter GC, Ringer BE, et al. Alpha-synuclein immunopositive aggregates in the myenteric plexus of the aging Fischer 344 rat. Exp Neurol 2009;220:109–119.
41. Bu LL, Huang KX, Zheng DZ, et al. Alpha-synuclein accumulation and its phosphorylation in the enteric nervous system of patients without neurodegeneration: an explorative study. Front Aging Neurosci 2020;12:575481.
42. Camilleri M, Cowen T, Koch TR. Enteric neurodegeneration in ageing. Neurogastroenterol Motil 2008;20:185–196.
43. Schemann M, Camilleri M. Functions and imaging of mast cell and neural axis of the gut. Gastroenterology 2013;144:698–704.e4.
44. Hickman SE, Kingery ND, Ohsumi TK, et al. The microglial sensome revealed by direct RNA sequencing. Nat Neurosci 2013;16:1896–1905.
45. Gautier EL, Shay T, Miller J, et al. Gene-expression profiles and transcriptional regulatory pathways that underlie the identity and diversity of mouse tissue macrophages. Nat Immunol 2012;13:1118–1128.
46. Cserep C, Posfai B, Lenart N, et al. Microglia monitor and protect neuronal function through specialized somatic purinergic junctions. Science 2020;367:528–537.
47. Norris GT, Smirnov I, Filiano AJ, et al. Neuronal integrity and complement control synaptic material clearance by microglia after CNS injury. J Exp Med 2018;215:1789–1801.
48. Preissler J, Grosche A, Lede V, et al. Altered microglial phagocytosis in GPR34-deficient mice. Glia 2015;63:206–215.
49. Zhan Y, Paolicelli RC, Sforazzini F, et al. Deficient neuron-microglia signaling results in impaired functional brain connectivity and social behavior. Nat Neurosci 2014;17:400–406.
50. Stevens B, Allen NJ, Vazquez LE, et al. The classical complement cascade mediates CNS synapse elimination. Cell 2007;131:1164–1178.
51. Pendse M, Li Y, Salinas CN, et al. Macrophages regulate gastrointestinal motility through complement component 1q. bioRxiv, 2022.
52. Deczkowska A, Keren-Shaul H, Weiner A, et al. Disease-associated microglia: a Universal immune sensor of neurodegeneration. Cell 2018;173:1073–1081.
53. Jump RL. Clostridium difficile infection in older adults. Aging Health 2013;9:403–414.
54. Liddle RA. Parkinson's disease from the gut. Brain Res 2018;1693:201–206.
55. Challis C, Hori A, Sampson TR, et al. Gut-seeded alpha-synuclein fibrils promote gut dysfunction and brain pathology specifically in aged mice. Nat Neurosci 2020;23:327–336.
56. Devos D, Lebouvier T, Lardeux B, et al. Colonic inflammation in Parkinson's disease. Neurobiol Dis 2013;50:42–48.
57. Choi I, Zhang Y, Seegobin SP, et al. Microglia clear neuron-released α-synuclein via selective autophagy and prevent neurodegeneration. Nat Commun 2020;11:1386.

Received August 11, 2022. Accepted September 15, 2022.

Correspondence:
Address correspondence to: Laren Becker, MD, PhD, Medicine/Gastroenterology, Stanford University, 300 Pasteur Dr., Alway Bldg, M215, Stanford, California 94305. e-mail: lsbecker@stanford.edu.

Authors' Contributions:
Laren Becker and Aida Habtezion designed the research; Madison McCarthy, Leila Neshatian, and Brooke Gurland identified study patients and provided tissue and clinical data; Laren Becker, Estelle Spear Bishop, and Hong Namkoong performed the research; Laren Becker, Estelle Spear Bishop, Laure Aurelian, Pratima Nallagatla, and Wenyu Zhou analyzed the data; Laren Becker, Estelle Spear Bishop, and Laure Aurelian wrote the paper.

Conflicts of Interest:
The authors disclose no conflicts.

Funding:
This work was supported by National Institutes of Health grants DK103966 and AG068394 to L.B. and AG049622 to A.H.

Ethical Statement:
The corresponding author, on behalf of all authors, jointly and severally, certifies that their institution has approved the protocol for any investigation involving humans or animals and that all experimentation was conducted in conformity with ethical and humane principles of research.

Data Transparency Statement:
Data, analytic methods, and study materials will be made available to other researchers after contacting the corresponding author.

Reporting Guidelines:
ARRIVE.